Eur. Phys. J. AP **11**, 59–69 (2000)

THE EUROPEAN PHYSICAL JOURNAL APPLIED PHYSICS

Transition from diffuse to constricted low current discharge in argon

S. Živanov, J. Živković, I. Stefanović[a], S. Vrhovac, and Z.Lj. Petrović

Institute of Physics Belgrade, Pregrevica 118, POB 68, 11080 Zemun Belgrade, Yugoslavia

Received: 20 March 2000 / Revised and Accepted: 25 May 2000

Abstract. We have measured the basic characteristics of low current diffuse discharges in argon for low pressures. The data for the voltage current characteristics and negative differential resistance were obtained together with the data for the frequency and for the damping coefficient of the induced oscillations. These data were compared with the predictions of a simple analytic model of Phelps, Petrović and Jelenković [A.V. Phelps, Z.Lj. Petrović and B.M. Jelenković, Phys. Rev. E **47**, 2825 (1993)] and it was found that, while most observables may be represented correctly, there is a systematic discrepancy between the predictions for frequency of induced oscillations based on the data for transport coefficients from the literature and measurements. The basic idea of the present work is thus to check the fundamental assumptions of the theory and to extend the application of the experiment to study the transition to constrictions in order to initiate modifications of the theory to cover the transition to the constricted regime. Very good agreement was found between the spatial profiles of the electric field calculated from the model and the data obtained from the spatial profiles of emission and these data may be extended to follow the transition to the constricted regime and the development of the cathode sheath.

PACS. 52.80.Dy Low-field and Townsend discharges – 52.80.Hc Glow; corona – 52.40.Hf Plasma–wall interactions; boundary layer effects; plasma sheaths

1 Introduction

For a long time, it was considered that Townsend's theory [1] fully describes the low current non-self-sustained and self-sustained electrical discharges, *i.e.* the dark Townsend regime [2]. However, this theory cannot explain some phenomena that were observed in experiments [3–7] such as negative differential resistance, oscillations in current and voltage and the well known transition to constriction. The region where such phenomena occur was even labeled "subnormal". Recently, it became possible to develop corrections to the standard Townsend's breakdown theory in order to explain negative differential resistance and its relation to oscillations occurring for low current diffuse regime [3–7]. Consequently, the transition to the constricted regime became the subject of further studies [7–9]. In addition, the kinetics of the low pressure breakdown was found to deviate significantly, at most E/n (where E is electric field and n is the gas number density in units of Townsend $1Td = 10^{-21}$ V m^2), from the standard assumptions of the basic Townsend's theory [10].

Constriction is a phenomenon of transition from a region of diffuse to a region in which the higher current discharge operates in a narrow channel. This channel becomes wider with the increasing current. It is also necessary to mention that the transition to the normal glow (*i.e.* cathode fall formation) is not always accompanied by the appearance of constrictions.

Our interest in studies of development of constrictions at low pressures also comes from the fact that this phenomenon is one of the simplest forms of self-organization and that the reasons for the transition can be predicted on the basis of physics of low current diffuse discharges. Clearly, Townsend's theory in its basic form is not sufficient to achieve a totally adequate description, but some corrected forms of this theory may prove to be sufficient.

In this paper we describe the results of measurements in argon which enabled us to obtain well-defined experimental data for quantitative comparisons with the theories of diffuse low current discharges [3–7] and the theories of constriction that are being developed [8,11]. The data include measurements of volt-ampere characteristics, properties of the induced oscillations such as frequency and damping coefficient and radial and axial distributions of emission. From emission profiles we obtained axial distributions of electric field as the transition occurs from the uniform field distribution of the low current diffuse discharge to the highly non-uniform distribution of the constricted discharge.

The relevant literature, in addition to that already mentioned, may be separated into three categories. The

[a] e-mail: is@plas.ruhr-uni-bochum.de

first consists of papers associated with charge buildup in low current diffuse discharges [12] where it was shown that the space charge affects the discharge and causes it to depart from the basic assumptions of the Townsend's theory leading to the development of negative differential resistance and oscillations [13]. This group forms the foundation of the theory of Phelps and coworkers and have been reviewed more thoroughly in reference [3].

Another set of references important for the present work are those dealing with the development of the cathode fall. Recently, well defined measurements of the temporal development of the cathode fall were made in argon [14] and other gases. This paper gives an observation of how initially, as the pulse develops, the exponential growth starting from the cathode turns into the spatial profile peaking closer to the cathode with a well developed cathode fall and negative glow. However, in this paper temporal dependence of the voltage pulse had to be modified to promote mechanisms which dominate at low overvoltages, *i.e.* when the discharge is running. The present paper, deals with the similar development but observed in stationary, developed discharges and it is followed as a function of the increasing current.

Finally there are papers dealing with constrictions. Numerous references present experimental observations of constrictions under different conditions ranging from the results in dc discharges [15], in dc discharges in electronegative gases [16] to the constrictions in rf discharges [17] and also under the higher pressure conditions where thermal gradients may become the primary cause of constriction. In this paper we deal only with the simplest possible form of constrictions occurring at lower pressures and consequently higher E/n [7,18] where no thermal perturbation occurs in the gas and on the surface of the cathode. Theoretical descriptions of the transition from the low current diffuse to the constricted (normal) glow include those trying to predict the shape of the channel in imposed or self-consistently calculated field distributions by adding the radial fields and diffusion losses [19].

However, the onset of transition is determined by processes at low currents. Such discharges (*i.e.* operating in dark Townsend regime) may be described exactly by extending the simple Townsend theory and many aspects of the theory may be established by comparing the theoretical predictions and the measured, well defined, properties such as volt-ampere characteristics, oscillation frequencies and damping coefficients. Thus our point is that low current diffuse mode theories such as that of Phelps and coworkers [3] may be extended to predict the onset of transition to constrictions and its principal causes even without attempting to predict the exact properties of the constricted discharge itself.

Yamaguchi and Makabe [20] have used the bifurcation theory to solve the system of fluid equations for electrons and for the ions and obtain the transition to the glow described as a phase transition with the condition for the existence of the sudden transition (*i.e.* what appears to be like subnormal glow) given by the criterion that the second derivative of the effective ionization coefficient changes sign. Unfortunately their technique was applied to silane discharge only, where data are somewhat limited and there is a possibility of the existence of several different ions including negative ions. A much clearer picture of the correspondence between this model and our results including the proposed physical explanations [11] may be obtained if the model of Yamaguchi and Makabe is applied to argon. A similar technique was used by Ma ode [21] who applied thermodynamic techniques to de- scribe the transition as a condition for achieving optimal operating conditions.

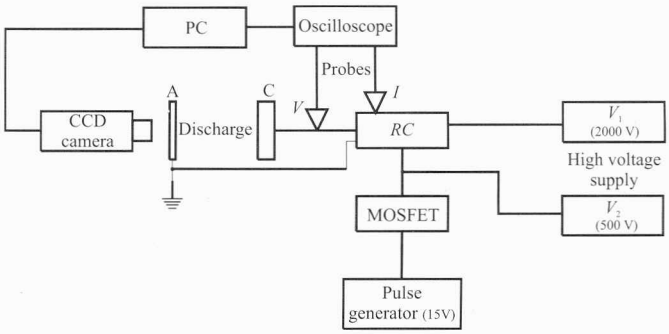

Fig. 1. Schematics of the experimental setup.

2 Experimental setup and procedure

The system that we use for our measurements in argon consists of parallel plate electrodes inside a quartz cylinder that prevents the long path breakdown. The copper cathode and the anode, which was made transparent by depositing a thin film of gold on quartz, can be positioned at several fixed distances, but it is necessary to open the system to adjust the gap. The diameter of the electrodes ($2r$) was 5.4 cm while the gap (z) was 1.0 cm. Recordings of axial and radial emission were made by a CCD camera. Our system is designed to make it possible to produce a pulse of current in addition to a very small dc current [1,4,5]. The dc current allows us to avoid long breakdown delay times [22]. The dc current is as small as possib in order to avoid heating and/or significant conditioning of the cathode during the measurements. It was necessary to treat the surface of the cathode from time to time by a relatively high current (30–100 μA) in a hydrogen discharge before the measurements in argon, in order to achieve a stable breakdown voltage. The schematic of the experiment is shown in Figure 1.

Gas flow is used to reduce the accumulation of impurities and products of the discharge. Voltage is measured by two probes connected as closely as possible to the anode and to the cathode, when a relatively high monitoring resistor is used in the low voltage anode circuit to determine the current. After a stable, low dc current operation is achieved, pulses of higher current are triggered lasting only long enough to achieve stable final discharge and to make reliable recordings of voltage and current transients. Operation in low duty cycle or single shot mode allowed

us to make measurements without modifying the surface of the cathode or heating the gas significantly [4–6].

3 Model of the low current discharge

The model that was used here is based closely on the phenomenological model of Phelps *et al.* [3] but we also use some of the results of the physical model. The basic assumption is that the negative differential resistance and consequently all other characteristics are caused by a small perturbation of the field due to space charge shielding of the external field. Thus it is essential to calculate the field distribution which provided motivation for us to make measurements presented here.

Within the framework of the phenomenological model of Phelps *et al.* it is possible to represent the physical processes with effective quantities, most importantly to use the negative effective resistance of the discharge R_{D}. According to the model of Phelps *et al.* the magnitude of the series resistor R_{S}, the stray capacitance C and relative magnitude of the monitoring resistor R_{m} and the discharge resistance R_{D} determine the behavior of the discharge current and the current stability regions [7]. The negative discharge resistance and other observables may be associated with the properties of the discharge itself such as the ion transit time T, the ionization coefficient α, the secondary electron yield γ and its dependencies on voltage $k_V = \partial\gamma/\partial V$ and on current $k_I = \partial\gamma/\partial I$. Thus the negative differential resistance of the discharge may be described by [3]:

$$R_{\mathrm{D}} = \frac{-k_I}{\gamma_{\mathrm{SS}}\,(\partial g/\partial V)}\left[1+\frac{I_{\mathrm{SS}}k_I}{\gamma_{\mathrm{SS}}(1+\gamma_{\mathrm{SS}})}\right] \times\left[1+\frac{I_{\mathrm{SS}}k_I}{\gamma_{\mathrm{SS}}(1+\gamma_{\mathrm{SS}})}\left[1-\frac{k_V}{\gamma_{\mathrm{SS}}\,(\partial g/\partial V)}\right]\right]^{-1}, \quad (1)$$

while the frequency of oscillations ω is given by

$$\omega^2 = \frac{I_{\mathrm{SS}}}{R_{\mathrm{S}}CT}\left[(R_{\mathrm{S}}+R_{\mathrm{m}})\frac{\partial g}{\partial V}-\frac{k_I}{\gamma_{\mathrm{SS}}}\right] \times\left[1+\frac{I_{\mathrm{SS}}(k_I-R_{\mathrm{m}}k_V)}{\gamma_{\mathrm{SS}}(1+\gamma_{\mathrm{SS}})}\right]^{-1}-k^2, \quad (2)$$

and the damping coefficient k is:

$$k = \frac{1}{2R_{\mathrm{S}}C}\left[1+\frac{I_{\mathrm{SS}}(k_I-(R_{\mathrm{S}}+R_{\mathrm{m}})k_V)}{\gamma_{\mathrm{SS}}(1+\gamma_{\mathrm{SS}})} -\frac{R_{\mathrm{S}}CI_{\mathrm{SS}}}{T}\left(\frac{k_I}{\gamma_{\mathrm{SS}}}-R_{\mathrm{m}}\frac{\partial g}{\partial V}\right)\right] \times\left[1+\frac{I_{\mathrm{SS}}(k_I-R_{\mathrm{m}}k_V)}{\gamma_{\mathrm{SS}}(1+\gamma_{\mathrm{SS}})}\right]^{-1}, \quad (3a)$$

or in a more simplified form:

$$k = \frac{1}{2R_{\mathrm{S}}C}+\frac{I_{\mathrm{SS}}}{2}(R_{\mathrm{m}}+R_{\mathrm{D}})\frac{\partial g/\partial V}{T}\cdot \quad (3b)$$

Here, I_{SS} is the "steady state" value of the discharge current (the value that discharge current reaches after a relaxation of the damped oscillations), C stands for stray capacitance and $\partial g/\partial V$ expresses the derivative of the round loop electron gain $g = \gamma(\exp(\alpha d)-1)$. As we can see from equation (3b) for $I_{\mathrm{SS}} = 0$ the damping tends to a constant value determined by the external circuit parameters.

Normalized negative differential resistance was also used for comparisons in the form [3]:

$$R_{\mathrm{N}} := \frac{A}{d^2}R_{\mathrm{D}} = -\frac{\hat{\gamma}f(\alpha d)}{\varepsilon_0 W_+\hat{g}}, \quad (4)$$

where A is the electrode area, W_+ is the ion drift velocity, ε_0 is dielectric constant of the vacuum, $\hat{\gamma}$ and $\hat{g}$ are the logarithmic derivatives of γ and g with the respect to E/n evaluated at E_0/n and $f(\alpha d)$ is a function of α and d in a form given in reference [3] (here E/n is the ratio of the electric field E to the gas density n, and E_0 is the value of the unperturbed electric field). Finally we calculate the field distribution from the equation for spatial distribution of ion density and Poisson equation (see Eqs. (37–44) in Ref. [3]).

The basis procedure was to apply the data for T and for α from the literature [3,7]. Ionization coefficient was parameterized by [7]:

$$\begin{aligned}\alpha/n = {} & 5\times10^{-21}\exp[-170/(E/n)] \\ & +3\times10^{-20}\exp[-700/(E/n)] \\ & +1.5\times10^{-20}\exp[-10^4/(E/n)]\end{aligned} \quad (5)$$

and used in the breakdown condition

$$\gamma_{\mathrm{SS}}[\exp(\alpha d)-1] = 1 \quad (6)$$

to determine the γ_{SS} coefficient by fitting it with:

$$\gamma_{\mathrm{SS}} = \gamma_{\mathrm{P}}+\frac{P\left(\dfrac{E/n}{Q}\right)^R}{1+\dfrac{E/n}{Q}}\cdot \quad (7)$$

Both our data and the data compiled by Phelps and Petrović [10] could be used in the analysis. In the analysis we used equation (7) with the best choice of parameters: $P = 3.4\times10^{-2}$, $Q = 2070\times10^{-21}$, $R = 1.1$ and $\gamma_{\mathrm{P}} = 0.001$. The value for k_V is obtained directly by differentiation ($\partial\gamma/\partial V$). The value for $\partial g/\partial V$ is obtained by differentiating g:

$$\frac{\partial g}{\partial V} = k_V(\exp(\alpha d)-1)+\gamma\frac{\partial\alpha}{\partial V}d\exp(\alpha d). \quad (8)$$

On the other hand k_I is obtained from:

$$R_{\mathrm{D}} = -\frac{k_I}{\gamma_{\mathrm{SS}}\partial g/\partial V}\cdot \quad (9)$$

Drift velocities of ions in a wide range of conditions (from 5×10^{-19} V m^2 to 1×10^{-16} V m^2) may be represented by:

$$W_+ = A\frac{E/n}{[1+B(E/n)^C]^D}, \quad (10)$$

where optimal values of parameters may be established by fitting the data from Table 8 in reference [23]: $A = 47$, $B = 2.1$, $C = 1.2$ and $D = 0.37$. These data were used to obtain the time of flight $T = \frac{d}{W_+}$ required in the formulae.

The calculated values of discharge parameters are shown in Table 1.

4 Results and discussion

Two sets of measurements were made. The first consisted of measurements of the properties of low current discharges in argon at different gaps d and fixed pd values. The measurement were performed in argon at low pressures ($pd = 40$ Pa cm, 66 Pa cm and 133 Pa cm [5,6] for different values of $d = 1-3$ cm). Low pressures were selected because, under those conditions, volt-ampere characteristic of the discharge allows us to probe the low current diffuse glow since negative differential resistance (NDR) is relatively low. Unfortunately, under those circumstances the constriction is not as sharp as that at higher pressures.

The second set of measurements was performed with a transparent electrode in order to observe constrictions and consequently the gap was somewhat different and fixed ($d = 1.1$ cm). It was possible to obtain constrictions at pressures of 133 Pa and 266 Pa.

At higher pressures it was not possible to record the properties of the discharge below the onset of constriction which required to correlate the measured conditions in the low current regime with the model in order to use the simple theory for that regime [3] to try to explain the non-linear effects leading to self-organization (*i.e.* constriction).

4.1 Volt-ampere characteristics and induced oscillations

It is important to measure the volt-ampere characteristics and properties of induced oscillations in order to establish the dominant feedback mechanism leading to the breakdown [3,5,6]. Our measurements of volt-ampere characteristics were presented earlier in reference [5] the results are in general agreement with those of Petrović and Phelps [7]. In the analysis of those characteristics it was found that the breakdown mechanism in argon might not be described purely by argon ion feedback mechanism (standard Townsend's theory) since the transit time of the ions does not correspond very well to the frequency of induced oscillations. In case of hydrogen the correspondence was excellent [3,5,6] but in the case of argon one may have to recognize the importance of additional mechanisms such as metastable and resonant photon induced breakdown [7,10].

In the following section we present a comparison of the measured current dependence of the volt-ampere characteristics, negative differential resistance, and also of the frequency and damping coefficient to the theoretical values calculated using formulae of the model [3,7]. In order

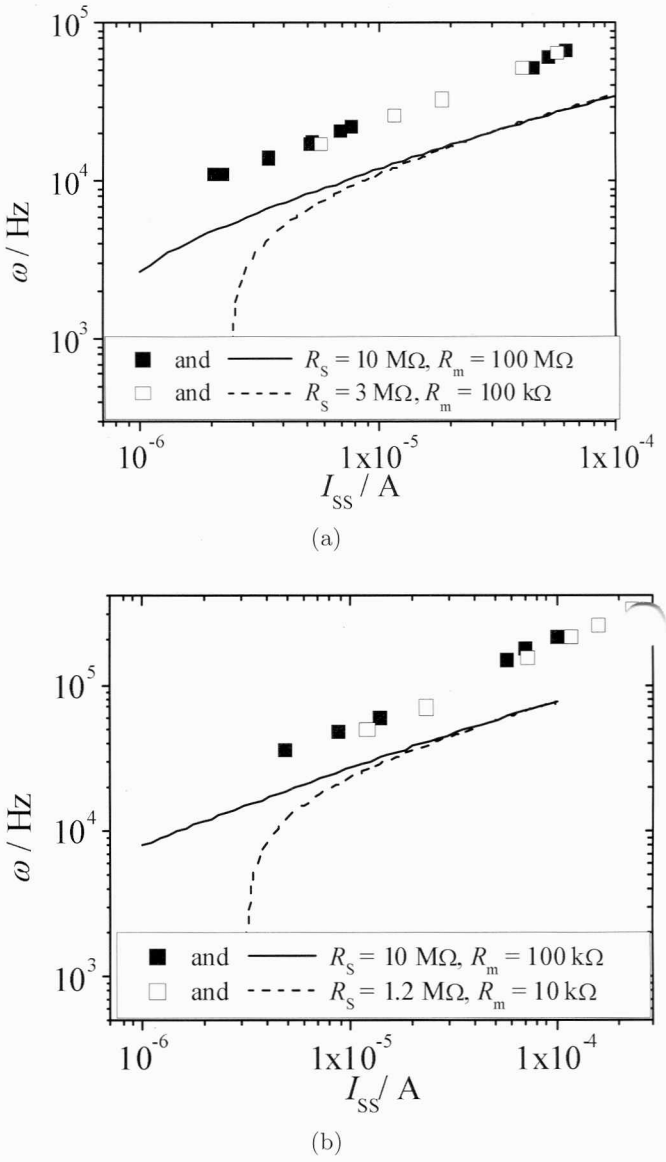

Fig. 2. Angular frequency of induced oscillations: a) $pd =$ 66 Pa cm, $d = 2$ cm; b) $pd = 133$ Pa cm, $d = 1$ cm. Points the experimental data obtained with different external circ... elements. Lines are predictions of the theory as explained.

to compare our results with the predictions of the model we had to use the discharge parameters obtained by fitting the model to our breakdown voltages and R_D values, in the manner proposed in reference [3].

In reference [5] we have shown several examples of the volt-ampere characteristics that were obtained in the first set of measurements. The characteristics obtained in the second set of measurements will be presented later associated with emission profiles. At this point we show in Figures 2 and 3 a few examples of the current dependencies of the frequency (ω) and of the damping constants (k), respectively. In these figures, the different data point-types represent the results of frequency and damping

Table 1. (a) Discharge parameters for argon, $pd = 40$ Pa cm, (b) discharge parameters for argon, $pd = 66$ Pa cm, (c) discharge parameters for argon, $pd = 133$ Pa cm, (d) discharge parameters for argon, $pd = 290$ Pa cm.

(a)

d (cm)	p (Pa)	V_B (V)	E/n ($\times 10^{-21}$ V m^2)	γ_{SS} ($\times 10^{-3}$)	R_D (kΩ)	T ($\times 10^{-6}$ s)	k_I (A^{-1})
1	40	690 ± 20	6990	31	-150	2.1	5.3
2	20	708 ± 40	7180	30	-440	4.1	15
3	13	714 ± 55	7240	30	-1100	6.1	35

(b)

d (cm)	p (Pa)	V_B (V)	E/n ($\times 10^{-21}$ V m^2)	γ_{SS} ($\times 10^{-3}$)	R_D (kΩ)	T ($\times 10^{-6}$ s)	k_I (A^{-1})
1	66	284 ± 16	1730	18	-150	4.5	14
2	33	309 ± 15	1880	16	-490	8.6	34
3	22	280 ± 1	1700	18	-1100	14	99

(c)

d (cm)	p (Pa)	V_B (V)	E/n ($\times 10^{-21}$ V m^2)	γ_{SS} ($\times 10^{-3}$)	R_D (kΩ)	T ($\times 10^{-6}$ s)	k_I (A^{-1})
1	133	228 ± 1	693	7.6	-180	7.5	22
2	66	242 ± 2	736	6	-520	14	51
3	44	223 ± 7	678	8.4	-1600	23	256
1.1	133	215 ± 1	580	7.55	-201	8.96	24

(d)

d (cm)	p (Pa)	V_B (V)	E/n ($\times 10^{-21}$ V m^2)	γ_{SS} ($\times 10^{-3}$)	R_D (kΩ)	T ($\times 10^{-6}$ s)	k_I (A^{-1})
1.1	266	212 ± 1	343	6.5	-370	12	25

easurements for different values of external circuit elements R_S and R_m.

We could not avoid the free running oscillations in argon for all discharge conditions under the conditions of the first set of experiments. The reason for this is that the value of the negative differential resistance is larger than the value of R_m (see Tab. 1). The measured angular frequencies and damping constants are compared to the model calculations in both figures. For the sake of simplicity we have omitted the dependence of measured frequencies on discharge circuit parameters that are much less important as compared to the case of damping coefficient. We have also omitted presenting the values of the oscillation frequencies in the current region of free running oscillations, because the model ceases to be valid for these conditions. The different types of data points are for different electrode spacing values and different line types are for the values predicted by the model of Phelps *et al.* [3].

4.2 Normalized negative differential resistance and discussion

We have also determined the values of negative differential resistance [3–5] by fitting the low current portion of the measured volt-ampere characteristics. To compare the measured values with the physical model (as described in the second Chapter of Phelps *et al.* [3]) we have used equation (4) and the results are shown in Figure 4. The breakdown voltage in argon discharge was stable so the estimated discharge parameter variation is of the order of the magnitude of the experimental points. For the model calculations there are two possibilities to obtain the data: one to fit the breakdown voltage and the other to use the values for $\hat{\gamma}$ and $\hat{g}$ derived from figures in the paper of Phelps and Petrović [7]. We have used the former approach, but both gave very similar results. The calculated value for R_N is practically independent of E/n, the same

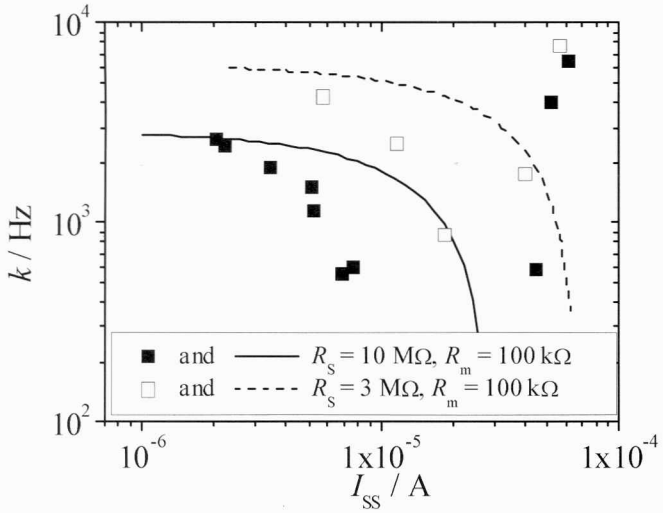

(a)

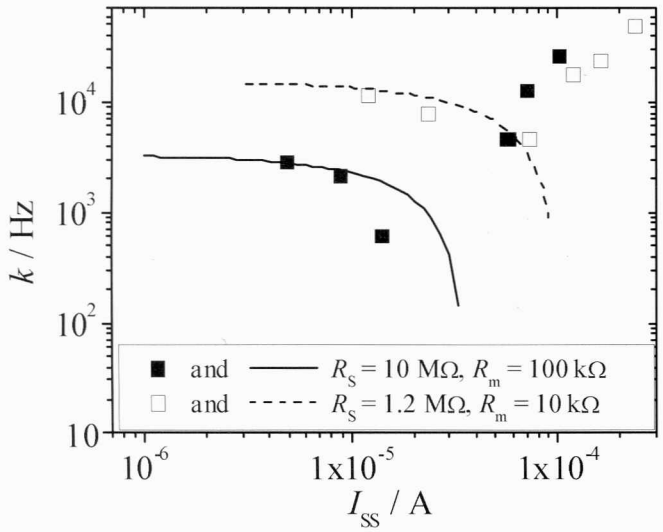

(b)

Fig. 3. Damping coefficient of induced oscillations: a) pd = 66 Pa cm, d = 2 cm; b) pd = 133 Pa cm, d = 1 cm. Points are the experimental data obtained with different external circuit elements. Lines are predictions of the theory as explained.

as in the experiment. On the other hand the calculated values of R_N are approximately three times larger than the experimental data. The results represented by crosses are the experimental values from [7] and are in good agreement with our experimental results.

We note that the frequencies predicted by the model are also systematically lower than the measured data. The discrepancy between the model and the experimental frequencies increases with increasing electrode distance, *i.e.* with lowering of the gas pressure for the same value of the normalized electrical field strength E/n. The discrepancies also increase with decreasing E/n.

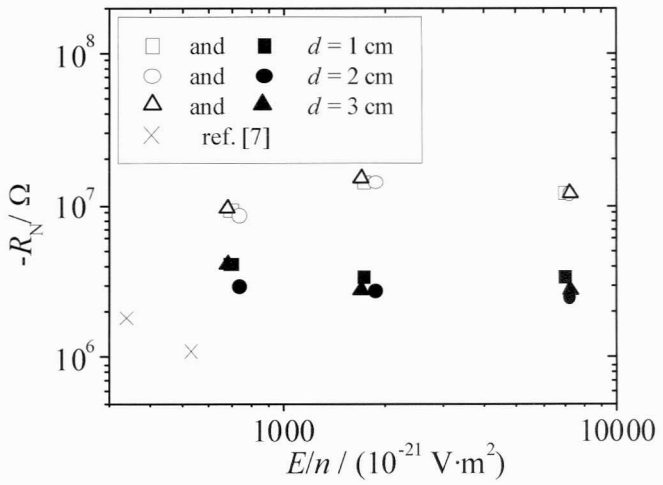

Fig. 4. Normalized negative discharge resistance R_N. Solid points are effective experimental data obtained for different geometries, open points are predictions of the model, crosses are the data of Petrović and Phelps [7].

If, however, we choose to increase the drift velocity of ions (*i.e.* the speed of feedback mechanism) by a factor of 2.5 a very good fit to all the experimental data is obtained. Even the fit for the damping constants is improved. The examples are shown in Figure 5 for properties of oscillations and Figure 6 for normalized negative differential resistance. This is consistent with the findings of Phelps and Petrović [10] that at moderate E/n, such as those covered here, ion feedback is not the dominant mechanism in breakdown and that photons from resonant states may make a significant, even determining contribution.

4.3 Radial and axial emission profiles

We have studied the initial stages of the transition from diffuse to constricted discharge by observing the profiles of emission. At low values of pd, covered below, constriction was not well established so we had to increase the pd value for these studies. At somewhat higher pd, however, it was not possible to perform measurements at different values of d due to a very high value of R_D. At pd = 133–146 Pa cm it was possible to do both measurements and the basic characteristics of the discharge used for constriction measurements (with somewhat larger distance between the electrodes) agree very well with the previously measured data (as shown in the separate row of Tab. 1c). The basic characteristics of the discharges used for field measurements at pd = 290 Pa cm are shown in Table 1d.

Measurements were made of both axial and radial profiles of emission. It is in principle possible to normalize the profiles to absolute values by using separately established profiles for specific lines and the data for excitation coefficients measured in a separate, absolutely calibrated system [25] but we have not done that since our data were not spectrally resolved. In separate experiments [25,26] it was shown that spatial profiles of the lines contributing

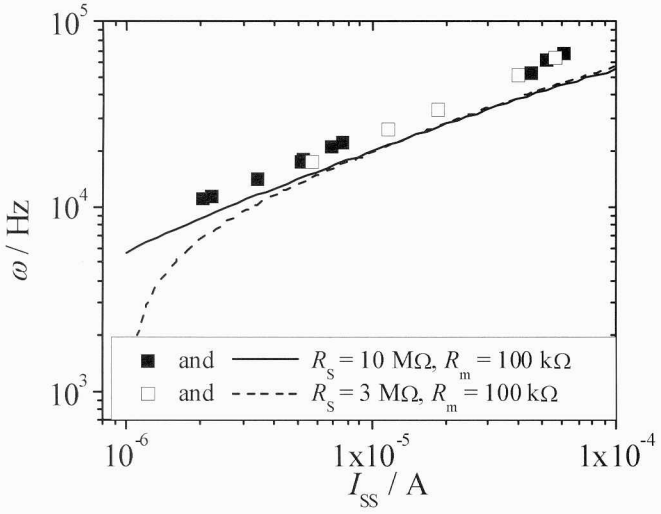

(a)

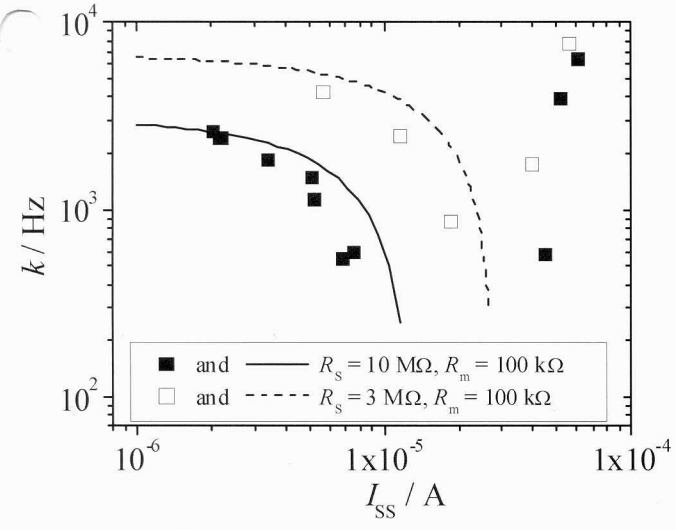

(b)

Fig. 5. Properties of induced oscillations calculated with arbitrarily increased drift velocity of ions by a factor of 2.5: frequency of oscillations: a) pd = 66 Pa cm, d = 2 cm; damping constant: b) pd = 66 Pa cm, d = 2 cm.

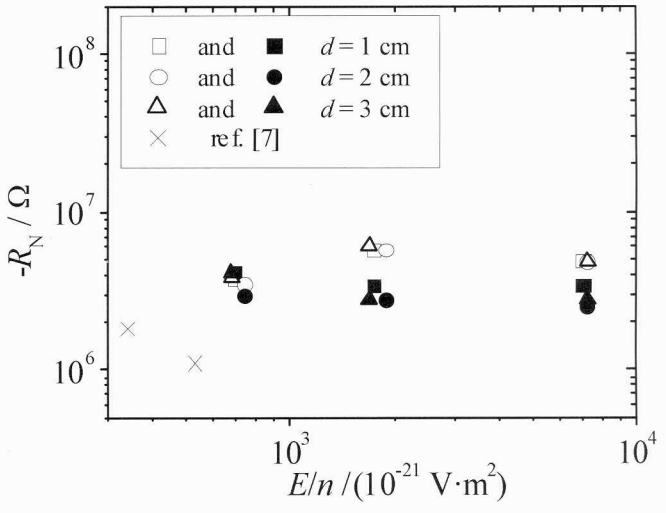

Fig. 6. Normalized negative discharge resistance R_N calculated with arbitrarily increased drift velocity of ions by a factor of 2.5. Solid points are effective experimental data obtained for different geometries, open points are predictions of the model, crosses are the data of Petrović and Phelps [7].

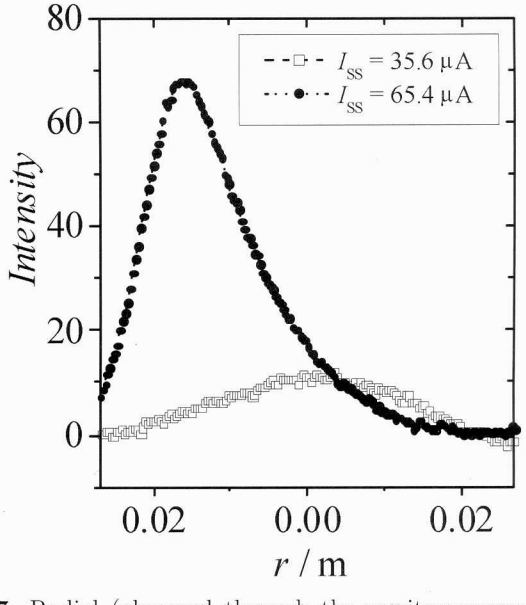

Fig. 7. Radial (observed through the semitransparent electrode) profiles of emission at pd = 290 Pa cm. The profiles were obtained at different currents where transition from a symmetric radial profile corresponding to the exponential axial profile to the asymmetric radial profile is observed.

most to the emission in visible and near infra red (where our CCD was sensitive) have the same spatial profiles with the same values of the corresponding ionization coefficient. The differences occur in the contribution of the heavy particle excitation which is developed as a peak close to the cathode [27–29] but we have not covered E/n values high enough to allow significant heavy particle excitation in determination of the profiles and field distributions.

We show radial (in Fig. 7) and axial (in Fig. 8) profiles in argon for pd = 290 Pa cm for different discharge currents. We have chosen this pd value because the constriction is more pronounced at higher pressures. At low currents, it is possible to describe the radial profile of emission by a zero order Bessel function [8]. As the current is increased, the profile is not symmetric anymore and the maximum of emission is moved from the center of the electrode. It means that the discharge changed its mode from a diffuse to the constricted. However, E/n is still high enough so that a very narrow constriction does not form. As mentioned above we were not able to make measurements below the onset of constriction under conditions when narrow channel forms (*i.e.* at higher pressures). At

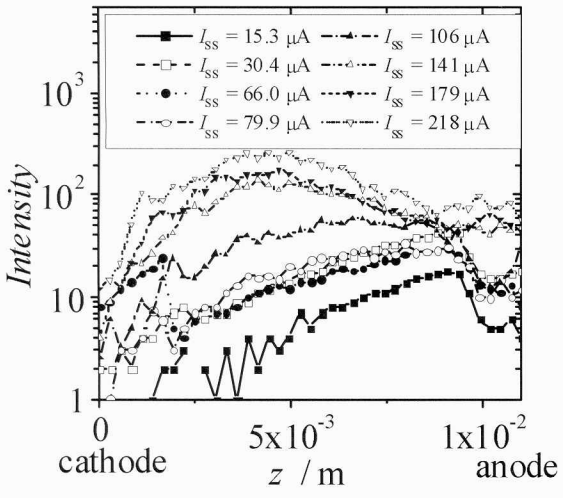

Fig. 8. Axial (along the axis of electric field) profiles of emission at $pd = 290$ Pa cm. The profiles were obtained at different currents where transition from a symmetric radial profile corresponding to the exponential axial profile to the asymmetric radial profile is observed.

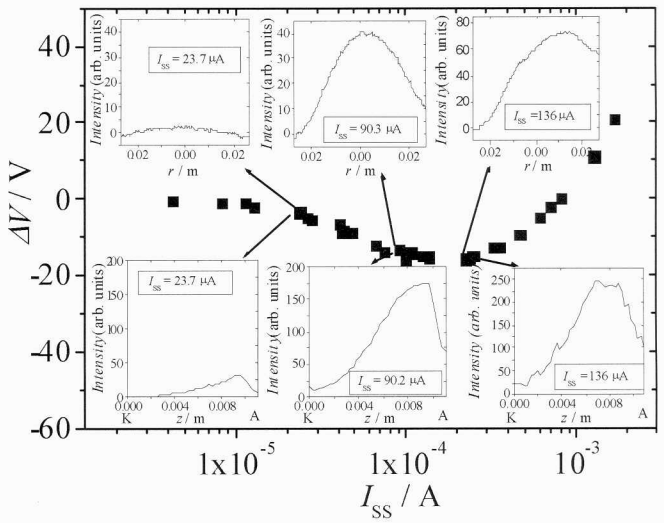

Fig. 9. Volt-ampere characteristic of the discharge in argon operating at $pd = 146$ Pa cm indicating the positions corresponding to different axial and radial profiles.

even higher currents the discharge extends to fill the whole radius again.

The exponential emission profiles along the field axis which are observed at low currents (Fig. 8) change significantly as current increases. Axial profiles at low current could only be measured down to $I_{SS} = 20$ μA as the sensitivity of the camera did not allow recording at lower currents without significant noise. At the lowest current covered here the profile consists of a broad non-equilibrium region next to the cathode and the growth of emission which for the lowest currents appears to be exponential. We have performed similar measurements in a different apparatus [26] where very low currents and the emission could be resolved spectrally. Under those conditions it was clearly established that at very low current a single exponential profile is observed changing slightly close to the anode as the current increases [30].

Close to the anode leveling off and decreasing of emission occurs due to poor resolution of the CCD and in that region one cannot establish the emission profile very accurately. In the region of emission growth there are at least two different exponentials that describe the growth at the lowest current covered here (see Fig. 8). At higher currents the profile of radiation has a rapidly changing slope and it levels much further from the anode indicating low electric field. Thus the profile is consistent with the development of the cathode fall and low field beyond it. At the highest currents there is very little change of the profile as the current increases and we did not carry the measurements further to reduce the need to clean the glass from the products of sputtering.

At the same time as the axial profiles make the change from exponential growth to a sudden growth and a broad peak, the radial profiles make transition from the centered Bessel function-like distribution to the narrower off-center distribution corresponding to the constriction. The fact that at low currents the distribution is centered indicates that the electrodes are very parallel. We use the radial profiles as a test of how parallel the electrodes are. In case that they are not, to the left of Paschen minimum the low current discharge will be confined to one end (longer distance) while to the right of Paschen Minimum the discharge would be confined to the opposite end (shorter distance). When discharge is centered in both cases the electrodes are sufficiently parallel.

The development of constriction in our experiment is followed to very high currents when the discharge fills the whole volume again. The correlation between the emission profiles and the volt-ampere characteristic is shown in Figure 9. We have not observed the rotating constrictions reported by Petrovic and Phelps [7] but sometimes the constrictions moved suddenly. One may observe that skewing of the axial field occurs first without constriction and that that only at higher currents when skewing of the field becomes significant, the transition to asymmetric radial profile occurs.

It is important to note that under some conditions a slow, gradual, transition to the final mode was achieved. In other words we were able to follow the transition to constricted mode without a sudden transition or even development of oscillations. However, one should note that in our procedure we make discrete changes to the current pulses and there is a possibility that such transition may occur though it may be quite small. At such values of pd as those covered here the voltage drop in transition to the constricted mode would be very small or negligible and negative differential resistance very small and thus the electric circuit as used here may provide a continuous transition. When we changed the dc voltage manually no significant transition was observed either but we could not make recordings of the voltage and current under such mode.

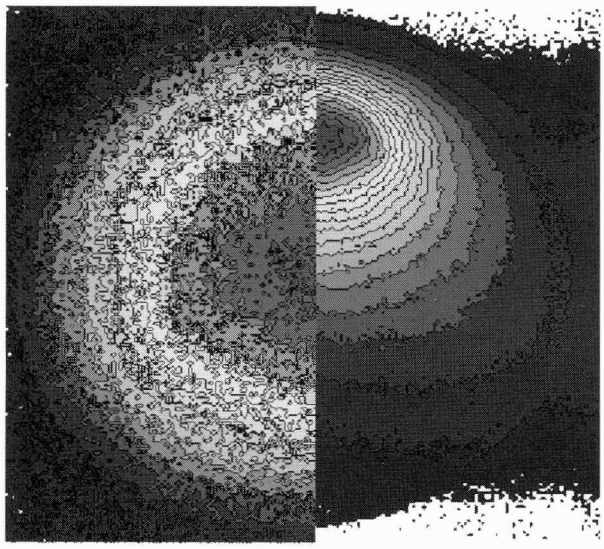

Fig. 10. Contour plots of radial emission profiles for conditions in Figure 7 (left: 36 μA and right: 65 μA at 290 Pa cm).

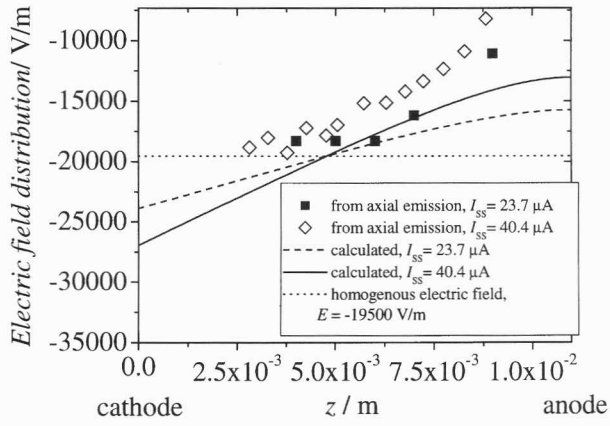

Fig. 11. Comparison between the theory and the model. Points are the measured field distributions obtained from the axial profiles for $pd = 146$ Pa cm and for two different currents: $I_{SS} = 23.7$ μA and $I_{SS} = 40.4$ μA. Lines are the calculated field distributions for the same currents and the homogenous electric field.

Finally we show the contour plot of the discharge for two similar currents below and above the onset of constriction in Figure 10.

4.4 Calculation of the field distribution

We were able to obtain the local field distribution from the experimental data by determining the slope of the emission profile and by associating it with the ionization coefficient from the literature [7,25,31] and also we have taken the local ionization coefficients to represent the fields. The choice of the regions which are fitted by a single exponential may be somewhat arbitrary. Nevertheless it is clear (see Fig. 8) that the slope changes sign and goes down towards the anode.

A comparison between calculated field distribution and that obtained from the axial emission profile is shown in Figure 11. The assumptions used in the analysis are valid in the region of swarm like transport, when the sheath is not formed, so the results obtained with the well developed sheath should be taken just as an indication. However, the data may be fitted by Monte Carlo simulations that would represent the non-hydrodynamic kinetics in the sheath [32].

In Figure 11 we can see the excellent agreement between the measured and calculated field distributions. Experimental data follow the basic characteristics of the profile predicted by the theory. At the highest currents covered in the experiment the calculation is not performed as the sheath is clearly developed which makes the model not valid as it is based on a small perturbation to the homogeneous field approximation. Yet we have observed a continuous transition and the charge induced field deviation becomes more and more pronounced leading to the development of the cathode fall. At lower currents we see the transition from approximately two to three distinct exponentials to several, the field becomes sharper and sharper with the increase of the current yet the overall voltage becomes smaller. The agreement between experimentally established field and the calculated values is very good except in the region of the plateau. Just where one should draw the limit of the region where leveling off does not affect the field determination is not clear so we have presented a broader range of the results rather than make an arbitrary division. It is however clear that leveling off at low current has one cause: the shadowing by the electrode while that at higher currents the low field region is clearly established as the plateau occurs quite far from the electrode. As the sheath is formed the accuracy of the field established from the emission profile may be questionable since the transport of electrons will be non-hydrodynamic (non-local). However, we have covered here the range which clearly includes conditions where such determination may be made. A gradual skewing of the field profile towards the well developed profile of the constricted (glow) discharge is observed sometimes without a sharp transition. The values of the field agree well with the level expected for the uniform field and with the degree of skewing of the field predicted by the model [3].

The independently made measurements allowing determination of the axial profiles at even lower currents of 1–20 μA (but without the radial profiles) made it possible to establish the low current limit where a single exponential is an excellent approximation and thus one could determine the profile of the efficiency of detection all the way to the anode. The lowest currents covered here, with the limit set by the CCD detection technique correspond to the situation where field still changes significantly and thus the spatial profile cannot be determined by a single exponential.

The field profiles determined here show symmetry, *i.e.* the point where field crosses the expected (uniform) value is quite close to the middle of the gap. The reason is that we operate in the region where ionization coefficient increases slowly, close to the point where the second

derivative of the ionization coefficient changes sign. That is the point of weak constriction and there, sudden transition to the constricted mode according to the theory of Yamaguchi and Makabe [20] is not expected.

5 Conclusion

In this paper we have recorded the basic data for low current discharges in pure argon. The data were measured to supplement the application of the models that are available with the specific idea that the model could be extended to predict the constrictions.

We recorded the voltage-current characteristics, negative differential resistance, the frequency and the damping coefficient of induced oscillations and also the characteristics of the self sustained oscillations. These data were compared with the predictions of the model of Phelps and coworkers which were found to give excellent agreement with the data for hydrogen when parameters taken from the literature were used. In argon however, there were some discrepancies, the same as reported elsewhere [7]. It was found that increasing the velocity of feedback particles from that of ions to 2.5 times larger gave excellent fit to all the data. Thus it is clear that the existing model [3] may need some corrections, in particular adding of the effect of resonance photons as suggested in references [7,10]. Nevertheless, the agreement between predictions of the model and the experimental results is still sufficiently good and much better than the agreement of other available analytical models, certainly much better than the direct and uncorrected application of Townsend's theory.

Radial profiles of emission and axial profiles of emission were also recorded for two values of pressure and for one distance between the electrodes. We have applied a CCD for recording the radial (through the anode) and axial (lateral to the discharge) profiles of emission. The correlation between these results and current-voltage characteristics was made.

Under the conditions of our experiment in low current discharge the radial profile of emission is centered and it is determined by the radial diffusion, so it has a profile of a Bessel function [8]. At the same time, the axial profile shows exponential growth toward the anode.

In the high current mode of operation the development of constriction is observed. It is quite wide due to the low pressure, but it is not symmetric. The axial profile shows a dark zone by the cathode, negative light and another dark zone close to the anode. In our experiment, there was not enough length for positive column to be developed. By choosing proper elements of electrical circuit we were able to observe a gradual transition from one regime to the other without the development of free running oscillations or sudden transition. Our conclusion is that the predictions of the simple one dimensional theory of Phelps and coworkers [3] gives good values of the field profile as compared to the values obtained from the slope of the emission profiles. In addition we may conclude that our results support directly the basic assumptions of the theory that the space charge induced field perturbation leads to the negative differential resistance and eventually to the development of the cathode sheath.

References

1. For example: S.C. Brown, *Introduction to Electrical Discharges in Gases* (John Wiley and Sons, New York, 1966).
2. Recently A.V. Phelps has recommended a constant terminology to label different regimes of low current discharges. Thus he proposed to use: low current diffuse (Dark or Townsend and subnormal), constricted glow (normal glow) and high current diffuse glow (abnormal) discharge. In this paper we shall mostly use this terminology, using the standard terminology only to make direct references that should be made without uncertainty.
3. A.V. Phelps, Z.Lj. Petrović, B.M. Jelenković, Phys. Rev. E **47**, 2825 (1993).
4. Z.Lj. Petrović, A.V. Phelps, Phys. Rev. E **47**, 2806 (1993); B.M. Jelenković, K Rózsa, A.V. Phelps, Phys. Rev. E **47**, 2816 (1993).
5. I. Stefanović, Z.Lj. Petrović, Jpn. J. Appl. Phys. **36**, 4728 (1997).
6. Z.Lj. Petrović, I. Stefanović, S. Vrhovac, J. Živković, J. Phys. IV France **C4**, 3412 (1997).
7. Z.Lj. Petrović, A.V. Phelps, Phys. Rev. E **56**, 2806 (1997).
8. V.I. Kolobov, A. Fiala, Phys. Rev. E **50**, 3018 (1994); A. Fiala, L.C. Pitchford, J.P. Bouef, Phys. Rev. E **49**, 5607 (1994).
9. A.V. Phelps, *Proceedings of XXIII ICPIG, Toulouse, France, 1997*, pp. II-48.
10. A.V. Phelps, Z.Lj. Petrović, Plasma Sources Sci. Technol. **6**, R20-R44 (1999).
11. A.V. Phelps, 1993 (unpublished), Z.Lj. Petrović, 1994 (unpublished).
12. R.W. Crowe, J.K. Bragg, V.G. Thomas, Phys. Rev. **96**, 10 (1954); A.L. Ward, Phys. Rev. **112**, 1852 (1958); A.L. Ward, E. Jones, Phys. Rev. **122**, 376 (1961); I. Mustata, C. Biloiu, Contrib. Plasma Phys. **38**, 447 (1998); M. Nahemov, N. Wainfam, A.L. Ward, Phys. Rev. A **137**, 56 (1963); A.L. Ward, J. Appl. Phys. **33**, 2789 (1962); K.H. Shoenbach, H. Chen, G. Schaefer, J. Appl. Phys. **67**, 154 (1990); A. Dengra, J. Ballesteros, M.A. Hernandez, V. Colomer, J. Appl. Phys. **68**, 5507 (1990).
13. M. Hayashi, Y.Miyoshi, Bull. Nagoya Inst. Technol. **15**, 339 (1962); Z. Donko, J. Phys. D **32**, 1657 (1999).
14. B.M. Jelenković, A.V. Phelps, J. Appl. Phys. **85**, 7089 (1999).
15. E.I. Toader, J. Phys. D **28** (1995); Z. Donko, G. Bano, L. Szalai, K. Kutasi, K. Rózsa, M. Pinheiro, N. Pinhao, J. Phys. D **32**, 2416 (1999).
16. D.B. Ogle, G.A. Woolsey, J. Phys. D **20**, 453 (1987).
17. P. Vidaud, S.M.A. Durrani, D.R. Hall, J. Phys. D **21**, 57 (1988).
18. V.V. Vlasov, L.G. Guseva, B.N. Klarfeld, *Proceedings of the X ICPIG 1971*, edited by R.N. Franklin (Donald Parsons and Co, Oxford, 1971), p. 98.
19. General constriction theories: P.K. Milsom, J. Phys. D **29**, 403 (1996); N.N. Christov, Europhys. Lett. **36**, 687 (1996); G.M. Petrov, C.M. Ferreira, Phys. Rev. E **59**, 3571 (1999).
20. Y. Yamaguchi, T. Makabe, Jpn. J. Appl. Phys. **31**, L1291 (1992).

21. P. Moussou, E. Marode, J. Phys. D **25**, 1205 (1992).
22. V.Lj. Marković, Z.Lj. Petrović, M.M. Pejović, J. Chem. Phys. **100**, 8514 (1994); V.Lj. Marković, M.M. Pejović, Z.Lj. Petrović, J. Phys. D **27**, 979 (1994).
23. A.V. Phelps, J. Phys. Chem. Ref. Data **20**, 557 (1991); A.V. Phelps, J. Phys. Chem. Ref. Data **19**, 653 (1990).
24. I. Stefanović, Ph.D. thesis, Faculty of Electrical Engineering, University of Belgrade, 1999; I. Stefanović, Z.Lj. Petrović (unpublished).
25. Z.M. Jelenak, Z.B. Velikić, Z.Lj. Petrović, B.M. Jelenković, Phys. Rev. E **47**, 3566 (1993); J.V. Božin, Z.M. Jelenak, Z.V. Velikić, I.D. Belča, Z.Lj. Petrović, B.M. Jelenković, Phys. Rev. E **53**, 4007 (1996).
26. G.N. Malović, J.V. Božin, B.M. Jelenković, Z.Lj. Petrović, Eur. Phys. J. D **7**, 129 (1999).
27. A.V. Phelps, B.M. Jelenković, Phys. Rev. A **38**, 2975 (1988).
28. Z.Lj. Petrović, V.D. Stojanović, J. Vac. Sci. Technol. A **16**, 329 (1998).
29. A. Strinić, M.Sc. Thesis, Faculty of Electrical Engineering, University of Belgrade, 1999 (unpublished); A. Strinić, G. Malović, Z.Lj. Petrović (unpublished).
30. S. Živanov, A. Strinić, G.N. Malović, Z.Lj. Petrović, 1999 (unpublished).
31. A.A. Kruithof, Physica (Utrecht) **7**, 519 (1940).
32. J.P. Boeuf, E. Marode, J. Phys. D **15**, 2169 (1982).